OXFORD

Human Molecular Genetics, 2016, Vol. 25, No. 16 3524–3538

doi: 10.1093/hmg/ddw195
Advance Access Publication Date: 17 July 2016
Original Article

ORIGINAL ARTICLE

Cancer-associated isocitrate dehydrogenase mutations induce mitochondrial DNA instability

Joanne M. Kingsbury[1,†,*], Nachiketha Shamaprasad[1], R. Blake Billmyre[1], Joseph Heitman[1] and Maria E. Cardenas[1]

[1]Department of Molecular Genetics and Microbiology, Duke University Medical Center, Durham, NC, USA

*To whom correspondence should be addressed at: Joanne M. Kingsbury , The Institute of Environmental Science and Research, PO Box 29181, Christchurch 8540, New Zealand. Tel: +64-3-3510137; Fax: +64 3 351 0010; Email: joanne.kingsbury@esr.cri.nz

Abstract

A major advance in understanding the progression and prognostic outcome of certain cancers, such as low-grade gliomas, acute myeloid leukaemia, and chondrosarcomas, has been the identification of early-occurring mutations in the $NADP^+$-dependent isocitrate dehydrogenase genes *IDH1* and *IDH2*. These mutations result in the production of the onco-metabolite *D*-2-hydroxyglutarate (2HG), thought to contribute to disease progression. To better understand the mechanisms of 2HG pathophysiology, we introduced the analogous glioma-associated mutations into the $NADP^+$ isocitrate dehydrogenase genes (*IDP1*, *IDP2*, *IDP3*) in *Saccharomyces cerevisiae*. Intriguingly, expression of the mitochondrial $IDP1^{R148H}$ mutant allele results in high levels of 2HG production as well as extensive mtDNA loss and respiration defects. We find no evidence for a reactive oxygen-mediated mechanism mediating this mtDNA loss. Instead, we show that 2HG production perturbs the iron sensing mechanisms as indicated by upregulation of the Aft1-controlled iron regulon and a concomitant increase in iron levels. Accordingly, iron chelation, or overexpression of a truncated *AFT1* allele that dampens transcription of the iron regulon, suppresses the loss of respirative capacity. Additional suppressing factors include overexpression of the mitochondrial aldehyde dehydrogenase gene *ALD5* or disruption of the retrograde response transcription factor *RTG1*. Furthermore, elevated α-ketoglutarate levels also suppress 2HG-mediated respiration loss; consistent with a mechanism by which 2HG contributes to mtDNA loss by acting as a toxic α-ketoglutarate analog. Our findings provide insight into the mechanisms that may contribute to 2HG oncogenicity in glioma and acute myeloid leukaemia progression, with the promise for innovative diagnostic and prognostic strategies and novel therapeutic modalities.

Introduction

Heterozygous mutations in either the cytoplasmic isocitrate dehydrogenase *IDH1* or mitochondrial *IDH2* genes occur early in the disease process in >70% of grade II and III gliomas and secondary glioblastomas (1–4), and also at a high frequency in several other cancers including acute myeloid leukaemias (AML) (5–8), chondrosarcomas (9), enchondromas, and hemangiomas (10). The Idh1 and Idh2 isocitrate dehydrogenases catalyze the $NADP^+$-dependent oxidative decarboxylation of isocitrate to α-ketoglutarate, an intermediate in both the tricarboxylic acid (TCA) cycle and anabolic processes. Mutations most frequently occur at conserved arginine residues important for binding of isocitrate (11), including Idh1 R132, the corresponding Idh2 R172 residue, or Idh2 R140. These mutations lead to the loss of isocitrate dehydrogenase activity (2,12), and impart a conformational change in the enzyme, resulting in a novel gain-of-function NADPH-dependent reduction of α-ketoglutarate to produce the "onco-metabolite" *D*-2-hydroxyglutarate (2HG) (6,13). Tumours bearing Idh1 R132 mutations produce up to 100-fold increased concentrations of 2HG (13,14).

Elevated 2HG levels, as well as the reduced production and increased utilization of α-ketoglutarate, have been proposed to

[†]Present address: The Institute of Environmental Science and Research, Christchurch, New Zealand.
Received: April 15, 2016. **Revised:** June 16, 2016. **Accepted:** June 17, 2016

contribute to tumourigenesis conferred by *IDH* mutations via multiple mechanisms. Normal α-ketoglutarate levels are an important signal for maintaining low levels of hypoxia-inducible factor 1α (HIF-1α), the master angiogenesis pathway regulator (12,15–17). Furthermore, the NADPH produced by Idh1 catalysis plays a significant role in the regeneration of reduced glutathione, which is important for the control of oxidative damage caused by reactive oxygen species (ROS) (18–20). 2HG is thought to act as an inhibitory analog of α-ketoglutarate due to their similar chemical structures, and as a result competes for binding to Fe(II)/α-ketoglutarate-dependent oxygenases, including prolyl hydroxylases required for targeting HIF-1α for degradation (21), chromatin-modifying JmjC histone demethylases (22,23), and Tet2-mediated 5-methylcytosine hydroxylation (23,24). Accordingly, *IDH*-mutated tumours and cell lines are associated with a hypermethylation state (23–28), a common facet of cancers affecting chromatin structure and transcription factor binding, which results in gene silencing and chromosome instability (29,30). *IDH*-mutated tumours are also frequently associated with chromosome arm 1p/19q codeletions or *TP53* mutations (31–33), suggesting an increased mutation rate.

Isocitrate dehydrogenases are highly conserved structurally and functionally throughout eukaryotes (34). The model yeast *Saccharomyces cerevisiae* has four isocitrate dehydrogenases localized to different cellular compartments: $NADP^+$-dependent Idp1 (mitochondrial), Idp3 (peroxisomal), and Idp2 (cytoplasmic) (35–38), and an NAD^+-dependent (mitochondrial) enzyme composed of Idh1 and Idh2 subunits. In addition to different subcellular localizations, the Idp1, Idp2, and Idp3 isozymes differ with respect to kinetic properties (37), contributions to metabolism (37,39–41), and expression conditions (35,39,42,43). The *S. cerevisiae* (Sc) Idp1, Idp2, and Idp3 are highly similar to *Homo sapiens* (Hs) Idh1 and Idh2 (67, 60 and 59% amino acid identity between Sc Idp1, Idp2, and Idp3, and Hs Idh1, respectively), and the arginine residues corresponding to R100 and R132 in Hs Idh1 (Hs Idh2 R140 and R172) are conserved in the corresponding yeast orthologs (Fig. 1A and C) . Moreover, expression of the mammalian *IDH1* or *IDH2* genes complements Sc *idp2*Δ and *idp3*Δ, and *idp1*Δ mutant phenotypes, respectively (43,44). Therefore, the yeast *IDP* genes provide an excellent model to study the biological effects of *IDH* mutations occurring in human cancers. We developed a novel yeast model to elucidate the biological impact of the onco-metabolite 2HG. We show that tumour-specific mutations in the yeast $NADP^+$-isocitrate dehydrogenase genes also result in a high-level of 2HG production. Remarkably, expression of the mutated mitochondrial isoform $IDP1^{R148H}$ caused extensive loss of mitochondrial (mt) DNA and associated defects in the ability to respire, analogous to the Warburg effect in tumour cells. We identify roles for the retrograde response pathway, α-ketoglutarate levels, and iron homeostasis in controlling the observed 2HG-dependent mtDNA loss. Our findings are of interest in light of recent studies underscoring an upregulation of iron trafficking in glioma cells (45) and suggest that this mechanism could potentially result in mitochondrial (mt)DNA damage often observed in tumour cells (46–48).

Results

Introduction of cancer-associated mutations in the yeast isocitrate dehydrogenase (IDP) genes results in production of 2HG at high levels

To generate a yeast model to study the cellular effects of isocitrate dehydrogenase mutation and 2HG production, tumour-associated mutations were engineered at the amino acid residues analogous to human $Idh1^{R132}$ of the yeast mitochondrial ($IDP1^{R148H}$), cytoplasmic ($IDP2^{R132H}$, $IDP2^{R132C}$), and peroxisomal ($IDP3^{R132H}$) isocitrate dehydrogenase genes (Fig. 1A and C). Specifically, the mutant alleles were introduced at their endogenous location, in a haploid *S. cerevisiae* background, and placed under the control of the strong *GAL1* promoter (expression is induced in galactose and repressed in dextrose). Importantly, analysis of protein-normalized cell lysates showed that the P_{GAL1}-$IDP2^{R132C}$ and P_{GAL1}-$IDP1^{R148H}$ expressing strains produced approximately 52-fold and 88-fold higher 2HG levels than the wildtype (WT), respectively (Fig. 1D), as determined by LC-MS. Therefore, the expression of human cancer-associated isocitrate dehydrogenase mutants of yeast orthologs also results in high-level 2HG production in yeast cells.

Mitochondrial 2HG production results in loss of respiration and mtDNA

Interestingly, we observed a significant growth reduction (smaller colony size) following high level 2HG production by P_{GAL1}-mediated expression of the mitochondrial $IDP1^{R148H}$ gene, compared with the WT, and the *idp1*Δ, *idp2*Δ, and P_{GAL1}-$IDP2^{R132H}$ mutants (Fig. 1E). Furthermore, the 2HG-producing strains continued to exhibit a growth defect even following transfer from galactose media to dextrose media, which represses $IDP1^{R148H}$ expression and hence 2HG production (Fig. 2B). This indicates that 2HG causes permanent, inherited cell damage. The deleterious growth phenotype observed upon overexpression of the mitochondrial $IDP1^{R148H}$ allele is consistent with 2HG accumulation causing loss of respiratory function and mtDNA damage (petite phenotype). We therefore assessed if overexpression of $IDP1^{R148H}$ results in increased loss of respiration by comparing colony formation on media that allows differentiation between “grande” (respiration-positive) and “petite” (respiration-negative) colonies. As expected, we found no differences in petite formation between the WT, *idp1*Δ, and P_{GAL1}-*IDP1* strains following growth for 48 h in YPD (P_{GAL1} OFF) or YPGal (P_{GAL1} ON) media, or when P_{GAL1}-$IDP1^{R148H}$ strains were grown in YPD (Fig. 2A). In contrast, following a 48-h incubation of P_{GAL1}-$IDP1^{R148H}$ strains under inducing conditions (YPGal), approximately 95% of the resulting colonies were petite (Fig. 2A). Therefore, overexpression of the yeast mitochondrial isocitrate dehydrogenase containing a tumour-associated mutation that results in high-level 2HG production causes a loss in the ability to grow on non-fermentable carbon sources (respiration defect).

Loss of respiration can result from either minor mutations in certain nuclear or mitochondrial genes or partial to complete mtDNA loss. To determine if expression of $IDP1^{R148H}$ results in mtDNA mutation, we isolated DNA from ten variants that had lost respiration capacity following overexpression of $IDP1^{R148H}$ (2HG production) (Fig. 2B) and assayed them by PCR for the presence of two mtDNA genes that are distant from each other in the mitochondrial genome (*COX1* and *COX2*). While these genes were readily detected in the parental strains from which the petite variants were derived, they were absent in all 2HG-exposed petite strains tested (Fig. 2C). To further assess the extent of mtDNA loss, we microscopically examined DAPI-stained 2HG-exposed petite cells and strikingly, observed no DAPI-stained DNA colocalizing with mitotracker red-stained mitochondria in these cells (Fig. 2D). Finally, using whole genome sequencing analysis, we found that all of these respiratory-deficient isolates had undergone the complete loss of the mtDNA (Fig. 2E).

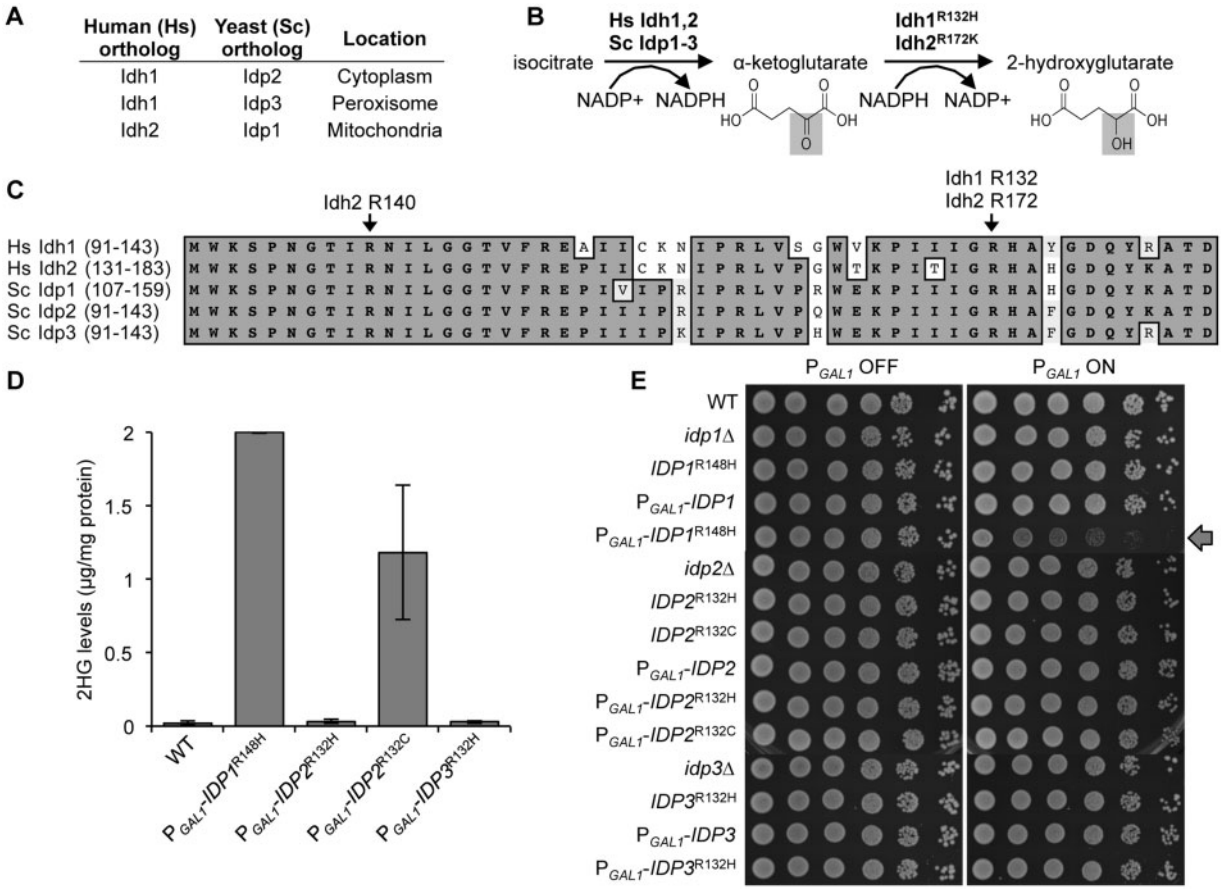

Figure 1. Introduction of tumour-associated mutations in yeast isocitrate dehydrogenase genes results in high-level 2HG production. (**A**) $NADP^+$-dependent isocitrate dehydrogenases in humans and yeast. (**B**) Biochemical reactions catalyzed by WT and mutant $NADP^+$-dependent isocitrate dehydrogenases. The chemical structures of 2HG and α-ketoglutarate are highly similar, differing only at the position indicated by shading. (**C**) Partial alignment of human (Hs) and yeast (Sc) $NADP^+$-dependent isocitrate dehydrogenases showing a high level of sequence identity and conserved arginine residues (depicted by arrows), which are mutated in various tumours. (**D**) Relative levels of 2HG from clarified extracts of cells incubated in YPGal for 6 h. The mean and standard deviation of duplicate measurements are shown; an independent experiment yielded similar results. (**E**) Growth phenotypes conferred by overexpression of the $IDP1^{R147H}$, $IDP2^{R132H}$, $IDP2^{R132C}$, and $IDP3^{R132H}$ alleles. Phenotypes were assayed following plating of 5 μl volumes of five-fold serially diluted cultures on SD + Ura (P_{GAL1}OFF) and SCGal + Ura (P_{GAL1}ON) media. Growth inhibition following induction of P_{GAL1}-$IDP1^{R147H}$ is depicted by an arrow.

Therefore, overexpression of $IDP1^{R148H}$ causes comprehensive loss of respirative capacity resulting from extensive loss of the mtDNA genome.

2HG production does not result in increased ROS or point mutation

Oxidative metabolism results in detrimental reactive oxygen species (ROS) in the mitochondria, which are particularly deleterious to mtDNA (49,50). NADPH, which is produced or consumed by WT or 2HG-producing isocitrate dehydrogenases, respectively, plays a significant role in the regeneration of reduced glutathione, important for control against oxidative damage caused by reactive oxygen species (ROS) (18–20). To investigate if 2HG production results in elevated ROS levels, we microscopically examined cells stained with the ROS-detection dye DCFH-DA, which is oxidized to the fluorescent chromophore 2-,7-dichlorofluorescein (DCF) in the presence of peroxide. As a positive control, we first showed that cells exposed to hydrogen peroxide resulted in a high proportion of fluorescing cells (Fig. 3A). We observed increased fluorescence in both the WT and P_{GAL1}-$IDP1^{R148H}$-expressing cells following 6 h induction consistent with an increased respiration capacity of cells grown with galactose as a carbon source (51). Fluorescence was reduced to background levels in both strains following 24-h incubation, and at each time point, no difference in the percentage of fluorescing WT and P_{GAL1}-$IDP1^{R148H}$ cells was observed (Fig. 3A). Therefore, 2HG production did not elevate ROS to levels detectable by this assay.

The superoxide dismutases Sod1 (cytoplasmic) and Sod2 (mitochondrial), and also glutathione (GSH) production, play key roles in the cellular defense mechanisms that protect against the deleterious effects of oxidative stress (52). However, high-copy expression of *SOD1* or *SOD2* or supplementation of cultures with GSH at different concentrations, did not suppress petite formation by the P_{GAL1}-$IDP1^{R148H}$ strain (Fig. 3B–D). Thus, these results are not consistent with a role for ROS in the observed petite formation.

The types of mutations occurring upon 2HG production could also provide insight into the mechanism of respiration loss. For example, if high 2HG levels result in the production of a mutagen that contributes to large-scale mtDNA loss, we might also predict an increased rate of point mutations in these strains. First, relative to the WT, *idp1*Δ mutant, and P_{GAL1}-*IDP1* strains, the P_{GAL1}-$IDP1^{R148H}$ 2HG-producing strain did not show a significant increase in the rate of nuclear DNA point mutation,

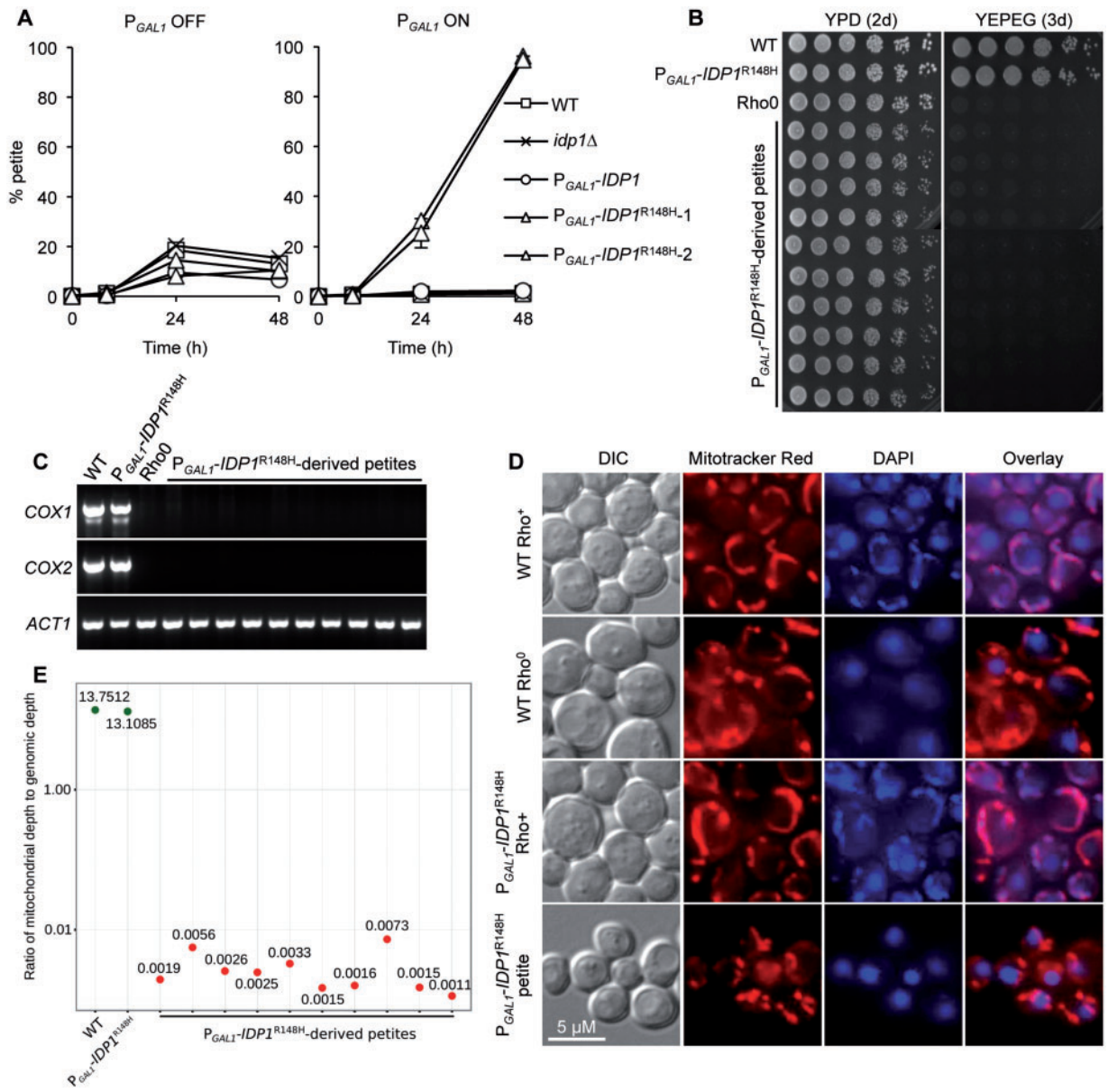

Figure 2. 2HG production by yeast mitochondrial isocitrate dehydrogenases induces extensive mitochondrial DNA loss. (**A**) The proportion of non-respiring (petite) cells in the strain populations was determined by dilution and plating onto YPGly 0.1% dextrose following incubation in triplicate in YPD (P_{GAL1} OFF) or YPGal (P_{GAL1} ON) for the times indicated. (**B**) Following growth of P_{GAL1}-$IDP1^{R148H}$ in YPGal, ten independently derived and presumptive petite isolates were plated onto YEPEG medium to confirm loss of respiration capability. Five μl volumes of 5-fold serial dilutions were plated on the indicated media and incubated for the time designated. (**C**) To determine the presence of mtDNA, total DNA was extracted from the ten petite mutants shown in (B), the grande WT and P_{GAL1}-$IDP1^{R148H}$ parent, and a Rho^0 strain and subjected to PCR using oligonucleotides specific for mitochondrially encoded *COX1* and *COX2* gene sequence, and the nuclear-encoded *ACT1* gene as a loading control. (**D**) Mitochondrial DNA was visualized by staining with DAPI (which also stains nuclear DNA) and mitochondrial localization was determined by staining with Mitotracker Red CMXRos. Results are presented for one petite isolate shown in (B), which was representative of all ten isolates. (**E**) Ratio of reads aligning to the mitochondrial genome as compared to the nuclear genome. Red circles indicate petite isolates derived from P_{GAL1}-$IDP1^{R148H}$, while green circles indicate strains with intact mitochondrial genomes. Virtually no mitochondrial sequence was detected in the petite strains sequenced in this study.

as determined by fluctuation analysis of mutation to canavanine resistance (Fig. 3E), which arises from point mutations in the *CAN1* arginine permease gene (53). Furthermore, 2HG-production did not elevate the mtDNA point mutation rate in grande cells (Fig. 3F), as determined by the acquisition of erythromycin resistance (Ery^R), which arises due to point mutations at several possible locations in the mitochondrial 21S rRNA gene (54,55). As shown previously, the spectrum of mutations occurring could also shed light on the mutational mechanism (56). We amplified and sequenced the Ery^R-relevant region of the 21S rRNA gene from 15 independently arising Ery^R mutants from both the WT and the 2HG producing strain following 24-h incubation in YPGal medium. However, we found a strikingly similar mutational spectrum between the WT and P_{GAL1}-$IDP1^{R148H}$ strain in this assay (Fig. 3G). Furthermore, we find no evidence of a high degree of point mutations occurring throughout the nuclear genome of nine petite variants that arose following overexpression of $IDP1^{R148H}$ (Supplementary Material,

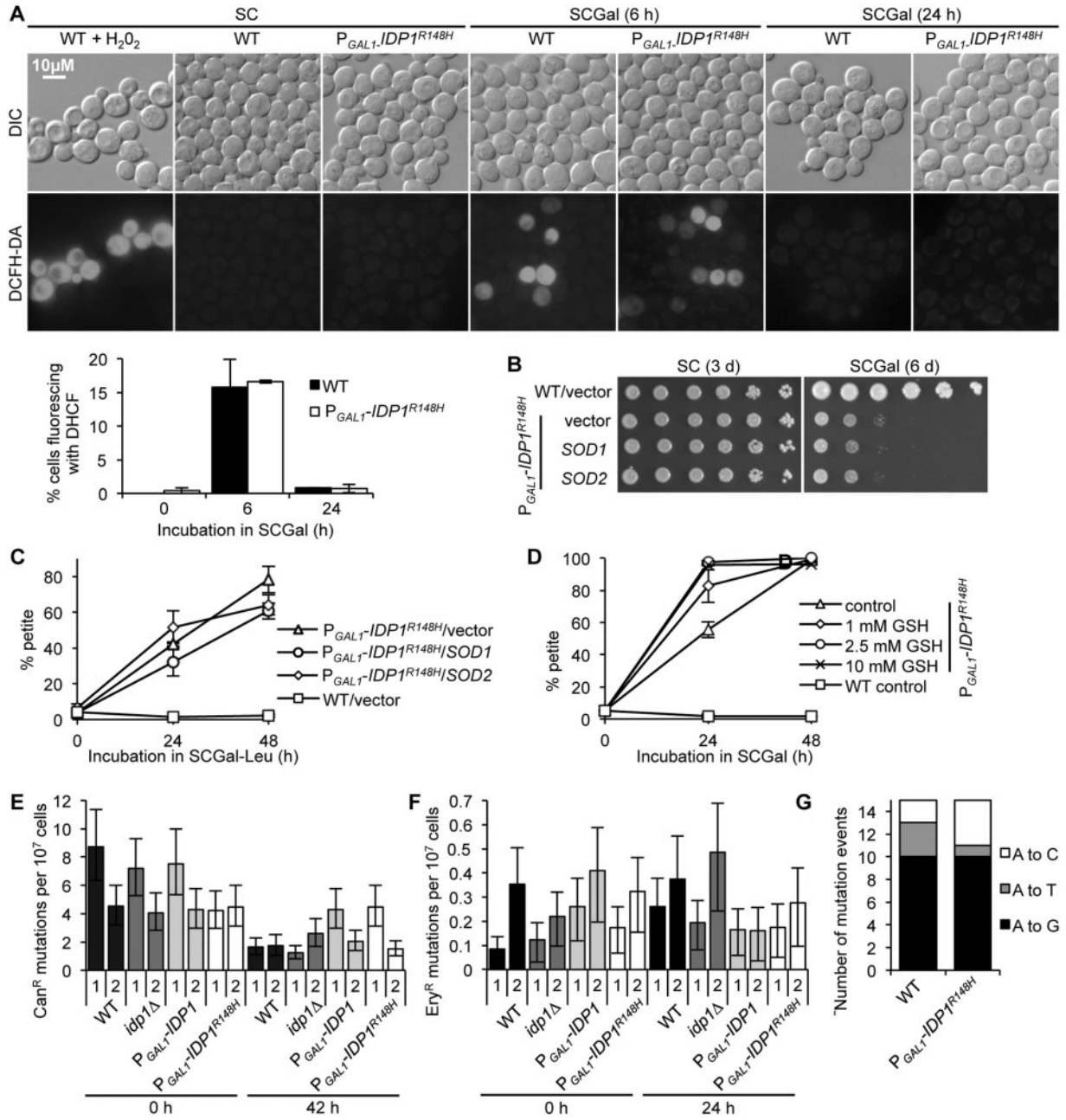

Figure 3. Mitochondrial 2HG production does not elevate ROS levels or the frequency of mitochondrial or chromosomal point mutations. (**A**) ROS production at time 0 (SC) and following 6 and 24-h induction of 2HG production by incubation in YPGal medium (P_{GAL1}-$IDP1^{R148H}$-ON) was visualized by fluorescence microscopy of DCFH-DA-stained cells. Cells treated with H_2O_2 (25 mM) for 1 hour prior to dye addition served as a positive control for ROS production (Note, due to the brightness of the fluorescent signal, the H_2O_2–treated cell image was captured with a shorter exposure time of 100 ms compared with 2 s for the other samples). More than 100 cells were counted from three separate fields of view at each time point, and results from duplicate cultures were averaged to determine the percentage of fluorescent cells. (**B, C**) The effect of *SOD1* and *SOD2* high-copy expression on petite formation was ascertained by (B) plating five-fold serial dilutions of the WT and P_{GAL1}-$IDP1^{R148H}$ strains transformed with the vector or high copy plasmids containing *SOD1* or *SOD2* onto SC or SCGal, or (C) by plating cultures incubated in SCGal-Leu onto YPGly 0.1% dextrose as described in Figure 2A. (**D**) The effect of reduced glutathione (GSH) on P_{GAL1}-$IDP1^{R148H}$-dependent petite formation was determined as described in Figure 2A following incubation in media supplemented with GSH at the indicated concentrations. (**E**) The rate of mutation to canavanine resistance as a measure of nuclear mutation rate was compared following growth in YPGal medium for 0 and 42 h. (**F**) The mutation rate to erythromycin resistance as an indicator for mitochondrial point mutation rate was determined following incubation in YPGal medium for 0 and 24 h. (E, F) Mutation rates from two independent experiments are shown. (**G**) The mutation spectrum was determined by sequencing the 1900-2000 region of the 21S rRNA gene of 15 independently isolated WT and P_{GAL1}-$IDP1^{R148H}$ erythromycin resistant isolates arising following incubation in YPGal for 24 h.

Table S4). In summary, 2HG production does not result in a significant increase of either nuclear or mitochondrial DNA point mutations.

ALD5 and *AFT1*$^{1\text{-}1207}$ are high-copy suppressors of 2HG-mediated mtDNA loss

To gain insight into the cellular processes involved in 2HG-mediated phenotypes, we sought to identify genes that, when expressed in high copy, suppress 2HG-mediated respiration loss. The P_{GAL1}-*IDP1*^{R148H} 2HG-producing strain was transformed with a high-copy number (average 10-20 plasmids/cell) yeast genomic library and Ura^{+} transformants were screened under P_{GAL1}-induction growth conditions (SCGal-Ura) for suppression of the deleterious 2HG-associated growth phenotype. We identified two suppressing genetic intervals. The first suppressing gene that was identified is *ALD5* (Fig. 4A and B), which encodes a mitochondrial aldehyde dehydrogenase that converts acetaldehyde to acetyl-CoA and participates in the breakdown of toxic aldehydes that accumulate during stress conditions (57). The second suppressing region comprised the first 1,207 bp of the 2,073 bp *AFT1* gene (Fig. 4A and B), a truncation allele of a transcription factor required for expression of high-affinity iron uptake (58,59). Interestingly, only the truncated allele (which lacks a glutamine-rich C-terminal domain thought to be required for transactivation (60)), but not the full-length *AFT1* gene, was capable of suppressing the 2HG-imposed growth defect (Fig. 4B). Consistent with the suppression of growth phenotypes on SCGal media, the high-copy number plasmids containing *ALD5* and *AFT1*$^{1\text{-}1207}$ also substantially suppressed petite formation of the P_{GAL1}-*IDP1*^{R148H} strain following P_{GAL1} induction (Fig. 4E).

To better understand the contributions of *ALD5* and *AFT1* to 2HG-induced mitochondrial DNA instability, we also investigated the phenotypes of strains disrupted for these genes in a WT or P_{GAL1}-*IDP1*^{R148H} background. Interestingly, P_{GAL1}-*IDP1*^{R148H} strains disrupted for *ALD5* (but not *ald5*Δ in an otherwise WT background) were respiratory-deficient, even prior to the induction of *IDP1*^{R148H} expression (see YEPEG plate in Fig. 4C). Strains mutated for *AFT1* were petite in both the WT (as reported previously from high throughput screens (61,62)) and *IDP1*^{R148H} backgrounds (Fig. 4C), consistent with a general role for Aft1 in respiration capacity.

We next ascertained whether overexpression of *AFT1*$^{1\text{-}1207}$ or *ALD5* in a P_{GAL1}-*IDP1*^{R148H} background affected levels of 2HG following P_{GAL1} induction for 6 h (SCGal-Ura). However, 2HG levels were just as high in extracts from these strains as they were from the P_{GAL1}-*IDP1*^{R148H} strain containing the vector control (Fig. 4D). Therefore, *AFT1*$^{1\text{-}1207}$ and *ALD5* do not suppress 2HG-mediated mtDNA loss by reducing 2HG levels via lower production or increased turnover.

Aft1 is known to interact with the ferrioxamine B transporter Sit1 (also known as Arn3), and certain Aft1 truncated forms similar to *AFT1*$^{1\text{-}1207}$ display increased Sit1-interaction together with increased ferrioxamine B transport, due to either enhanced Sit1 activity or reduced ubiquitin-mediated Sit1 proteolysis (63). However, we found that *AFT1*$^{1\text{-}1207}$ overexpression still suppressed petite formation in a P_{GAL1}-*IDP1*^{R148H} *sit1*Δ strain (Fig. 4B); thus, petite suppression by *AFT1*$^{1\text{-}1207}$ overexpression is not mediated via an effect on Sit1 function or stability. Given the role of Aft1 in iron homeostasis, we also tested if petite formation was altered by the addition of iron (II) or the iron chelator deferroxamine mesylate (DFO), which is transported by Sit1 (64). Petite formation was not suppressed by addition of either iron (II) or DFO at the concentrations tested (Fig. 4E). In contrast, chelation of iron from the SCGal growth medium with bathophenanthroline disulfonate (BPS, 100 μM) suppressed petite formation in a concentration-dependent manner (Fig. 4E).

Given the known role of Aft1 as a transcription factor, we assessed whether cells containing the high copy *AFT1*$^{1\text{-}1207}$ allele still sensed and upregulated the iron regulon in conditions of iron limitation. We compared the expression of the Aft1-regulated gene *FET3* (59, 60) in WT or P_{GAL1}-*IDP1*^{R148H} strains expressing the vector, high copy *AFT1*, or high copy *AFT1*$^{1\text{-}1207}$, grown in SC or SC treated with 100 μM BPS. First, in SC medium, *FET3* was expressed at similar levels both in the WT/vector and P_{GAL1}-*IDP1*^{R148H}/vector strains, and levels were doubled in the P_{GAL1}-*IDP1*^{R148H}/*AFT1* strain (Fig. 4F, first graph). Upon incubation of cells for 6 h in medium depleted for iron via BPS chelation, *FET3* expression was similarly induced approximately 6-fold compared with WT levels in SC medium in all three strains. Strikingly however, compared with the P_{GAL1}-*IDP1*^{R148H}/vector strain, *FET3* expression in the P_{GAL1}-*IDP1*^{R148H}/*AFT1*$^{1\text{-}1207}$ strain was approximately 12-fold (in SC medium) and 5-fold (in SC + BPS medium) lower, even though this strain still contained WT *AFT1* expressed from its endogenous location. Therefore, high copy expression of *AFT1*$^{1\text{-}1207}$ dampens expression of Aft1-regulated genes.

We also monitored *FET3* expression upon a shift into SCGal medium to induce 2HG production. Following 10-h incubation in SCGal medium, *FET3* expression in the P_{GAL1}-*IDP1*^{R148H}/vector strain was ∼2-fold elevated compared with the WT/vector strain (Fig. 4F, second graph). *FET3* levels in the P_{GAL1}-*IDP1*^{R148H} strain with high-copy *AFT1* expression remained 4 to 5-fold higher than for the P_{GAL1}-*IDP1*^{R148H}/vector levels at 10 and 24 h. Expression patterns observed at 10-h incubation in SCGal medium were similar to those observed for *FET3* as well as *FTR1* (also Aft1-regulated) at 6-h incubation in SCGal in an independent experiment (Supplementary Material, Fig. S1). In contrast, although *FET3* expression in the P_{GAL1}-*IDP1*^{R148H}/*AFT1*$^{1\text{-}1207}$ strain increased to levels comparable with the P_{GAL1}-*IDP1*^{R148H}/vector strain at early time points (6, 10 h) following a shift to SCGal (Fig. 4F and Supplementary Material, Fig. S1), this expression was dampened at T0 and later time points (24 h) (Fig. 4F). These results demonstrate that the *AFT1*$^{1\text{-}1207}$ allele dampens expression of the iron regulon most likely by the truncated Aft1 product competing with the endogenous WT Aft1 protein.

We next tested the effect of 2HG production and *AFT1*$^{1\text{-}1207}$ high-copy expression on whole cell iron content. The WT and P_{GAL1}-*IDP1*^{R148H} strains have equivalent iron levels during growth in SC medium (Fig. 4G, first graph). Remarkably, iron levels increased ∼2-fold higher in the P_{GAL1}-*IDP1*^{R148H} strain compared to the WT strain following induction of 2HG production in SCGal medium. However, these results are not accompanied by a predicted reduction of the *FET3* expression, which unexpectedly increased also by ∼2-fold (Fig. 4F). Alternatively, *FET3* upregulation is responsible for the increased iron observed in the P_{GAL1}-*IDP1*^{R148H} strain. Similar results were seen using the WT/vector and P_{GAL1}-*IDP1*^{R148H}/vector strains (Fig. 4G, second graph). Furthermore, high copy expression of *AFT1*$^{1\text{-}1207}$ (P_{GAL1}-*IDP1*^{R148H}/*AFT1*$^{1\text{-}1207}$ strain) resulted in 2.8-fold reduced P_{GAL1}-*IDP1*^{R148H} iron levels at 10 h in galactose medium as compared to the P_{GAL1}-*IDP1*^{R148H}/vector strain. In summary, our results suggest that 2HG production perturbs both iron homeostasis and possibly the iron sensing mechanism, and the resulting elevated cellular iron levels may contribute to the 2HG-dependent petite formation.

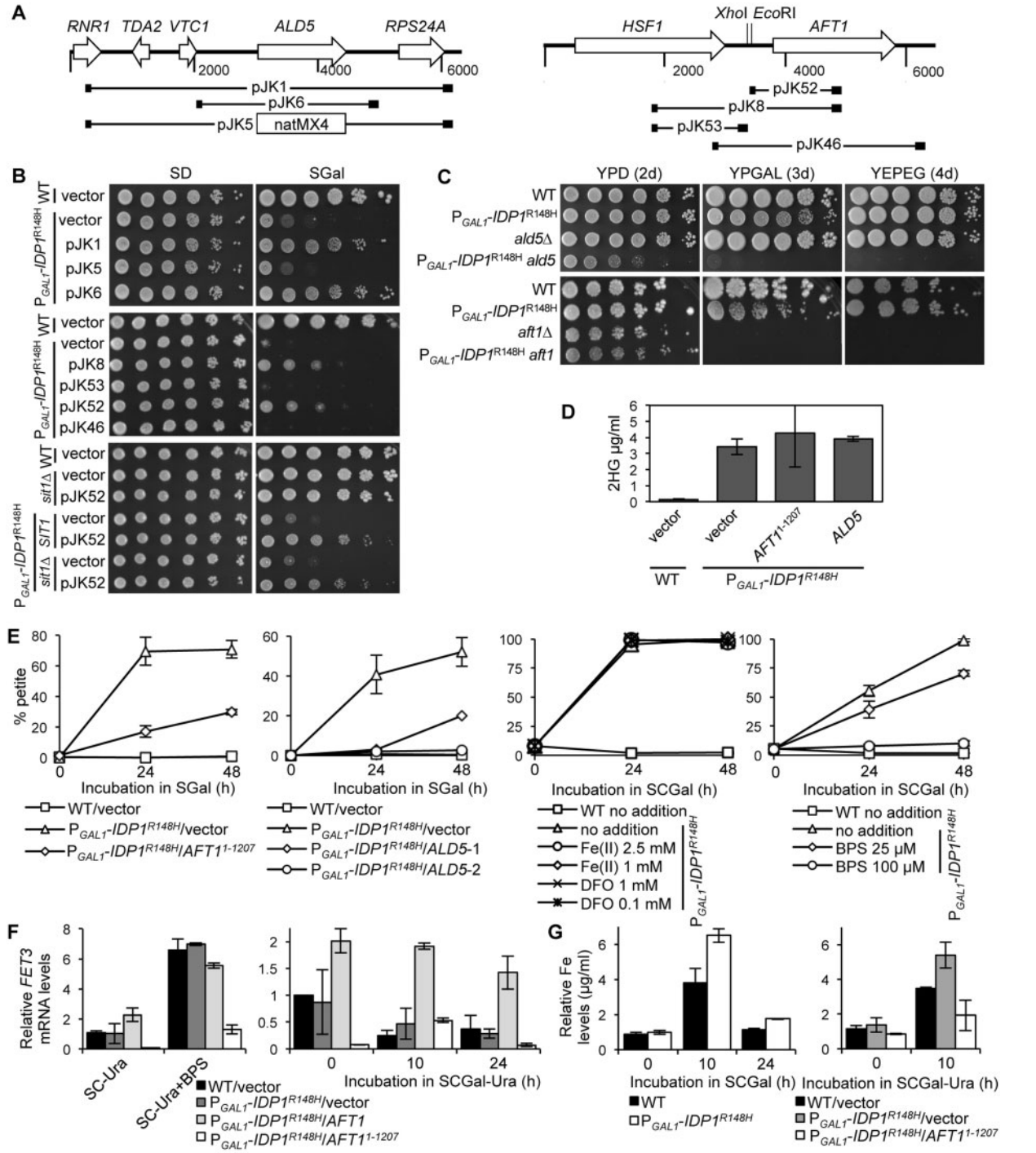

Figure 4. Overexpression of *ALD5* and *AFT1*$^{1\text{-}1207}$ suppresses the 2HG-mediated petite formation. (**A**) Genetic intervals of high-copy number plasmids that suppressed the P$_{GAL1}$-*IDP1*^{R148H}-mediated petite formation. (**B**) Five-fold serial dilutions of the WT, P$_{GAL1}$-*IDP1*^{R148H}, or P$_{GAL1}$-*IDP1*^{R148H} sit1Δ strains transformed with the vector or plasmids described in Figure 4A were plated onto SD (control) or SGal media to induce P$_{GAL1}$-*IDP1*^{R148H} expression and thereby 2HG production. (**C**) Five-fold serial dilutions of strains were plated onto the indicated media. (**D**) Relative levels of 2HG extracted from cultures grown in duplicate following incubation for 6 h in SCGal-Ura. (**E**) Suppression of petite formation was determined in triplicate by incubation of strains in SGal or SCGal media to induce 2HG production. Where indicated, media was supplemented with either no additions, individual additions of iron (II) sulfate heptahydrate (FeII), deferoxamine mesylate (DFO), or bathophenanthroline disulfonate (BPS). At the times indicated, cells were plated onto YPGly 0.1% dextrose media to determine the proportion of petite and grande colonies. (**F**) Quantitative RT-PCR measurements of *FET3* transcript levels relative to *ACT1*. RNA was extracted from strains grown in duplicate for 0 (SC-Ura), 10 or 24 h in SCGal-Ura, or 6 h following incubation in SC-Ura + BPS (100 µM). (**G**) Analysis of cellular iron content. Cells were grown in galactose medium for the times indicated, washed, and nitric acid cell extracts were analyzed for iron content by ICP-MS. Data shown is the average of three independent replicates. (D-G) Strains contained plasmids pRS426 (vector), pJK6 (*ALD5*), pJK52 (*AFT1*$^{1\text{-}1207}$), or pJK46 (*AFT1*).

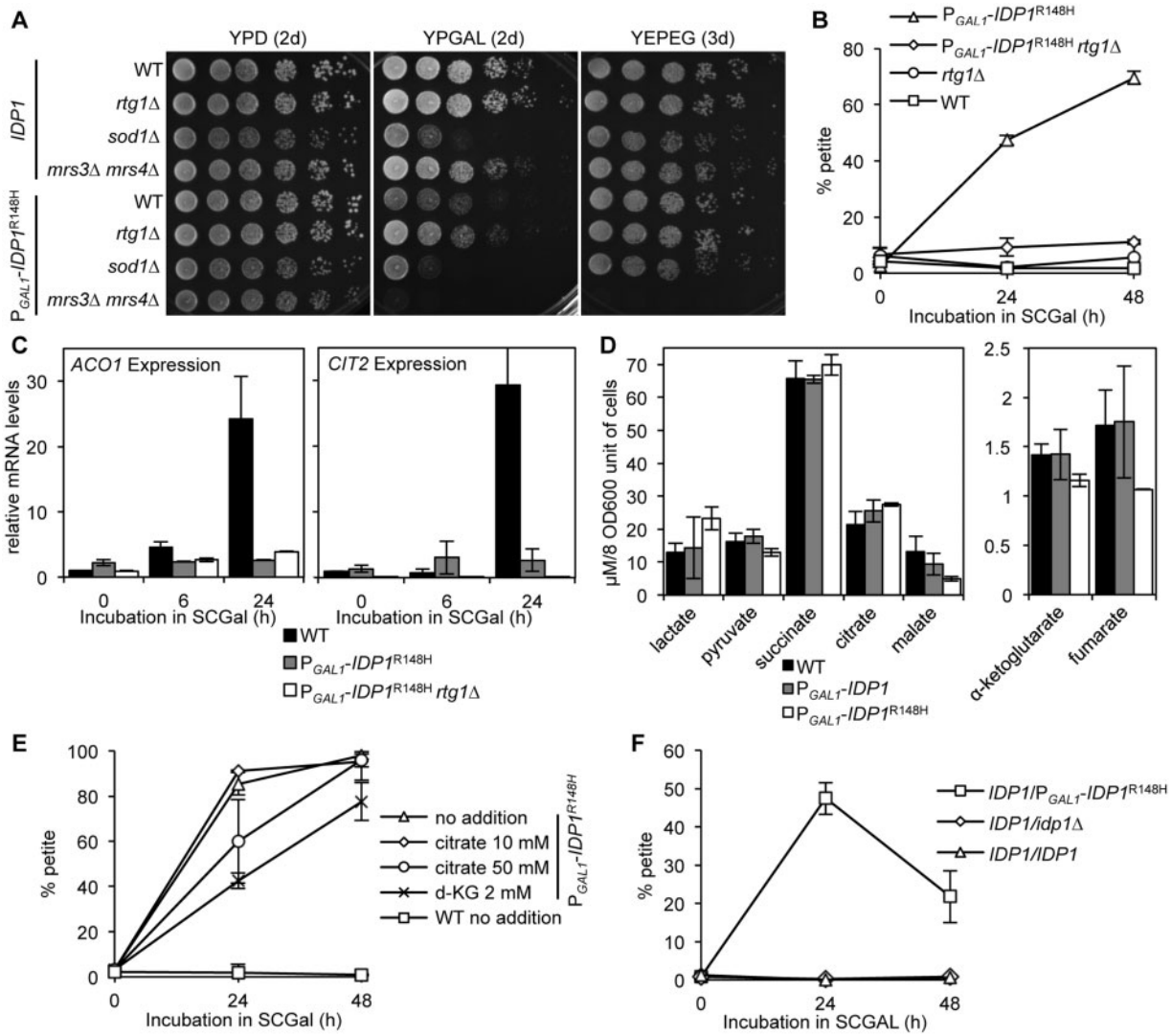

Figure 5. Mutation of *RTG1* or α-ketoglutarate addition suppress 2HG-mediated petite formation. (**A**) The WT *IDP1* or P_{GAL1}-$IDP1^{R148H}$ strains and their isogenic derivatives mutated for the genes indicated were cultured overnight in YPD, washed twice, serially diluted five-fold, plated onto YPD, YPGal, and YEPEG, and incubated for various times. (**B, E, F**) Triplicate cultures of strains were incubated in SCGal for the indicated times and plated onto YPGly 0.1% dextrose media to differentiate petite from grande colonies. For (E), strains cultured overnight in YEPEG were washed and inoculated in triplicate into SCGal, as indicated, with no additions, 10 or 50 mM sodium citrate, or 2 mM d-KG. (**C**) Quantitative RT-PCR measurements of *ACO1* and *CIT2* transcript levels relative to *ACT1*. RNA was extracted from strains grown in duplicate for 0, 6, and 24 h in SCGal-Ura. (**D**) TCA cycle intermediate levels extracted from strains incubated for 6 h in SCGal medium.

Retrograde pathway inhibition and α-ketoglutarate supplementation suppress 2HG-mediated petite formation

Interestingly, mutations in other TCA cycle genes have been shown to result in elevated mtDNA loss (65–67). Petite formation upon disruption of the aconitase gene *ACO1*, whose product is required to produce the IDP/IDH substrate isocitrate, has been attributed in part to activation of the retrograde pathway, which leads to increased citrate levels. In turn, increased citrate results in elevated levels of mitochondrial iron citrate, which reacts with hydrogen peroxide to form DNA-damaging hydroxyl radicals (68). We therefore tested whether a similar model also accounts for 2HG-mediated mtDNA loss. First, consistent with this model, we find that disruption of the gene encoding the retrograde pathway transcription factor *RTG1* substantially suppressed P_{GAL1}-$IDP1^{R148H}$ strain petite formation in galactose media (Fig. 5A and B). Mitochondrial dysfunction induces the retrograde (RTG) pathway (69). However, we did not find evidence of RTG pathway induction upon 2HG production, as the RTG-regulated genes *CIT2* and *ACO1* were not elevated following either 6 or 24-h incubation for the P_{GAL1}-$IDP1^{R148H}$ strain in galactose medium (Fig. 5C). Note that these genes were induced in the WT following a 24 hour incubation in SCGal; however, this was likely because at this time, the cultures had reached stationary phase unlike the slower-growing P_{GAL1}-$IDP1^{R148H}$ strain. Furthermore, levels of most TCA cycle metabolites, including citrate, were not elevated following P_{GAL1}-$IDP1^{R148H}$ induction relative to the WT and P_{GAL1}-*IDP1* strains (Fig. 5D and Supplementary Material, Table S5). Therefore, the *rtg1*Δ mutation appears to suppress 2HG-mediated petite formation by a mechanism independent from that mediating retrograde pathway suppression. Interestingly, suppression of petite formation by the *rtg1*Δ mutation was also not due to decreased 2HG

production as extracts from an P_{GAL1}-*IDP1*^{R148H} *rtg1*Δ strain had 2.5 higher 2HG levels than the P_{GAL1}-*IDP1*^{R148H} strain (5.0 and 2.0 μg/mg protein, respectively) following 6 h induction in galactose media. Moreover, *cit1*Δ mutation, which should reduce mitochondrial citrate levels, did not suppress 2HG-mediated petite formation (Supplementary Material, Fig. S2), and citrate supplementation instead partially suppressed petite formation (Fig. 5E). Finally, mutation of the mitochondrial iron transporter genes *MRS3* and *MRS4*, or of the superoxide dismutase gene *SOD1*, are all known to suppress petite formation of the *aco1*Δ strain (68). However, these mutations did not alleviate the petite formation phenotype of the P_{GAL1}-*IDP1*^{R148H} strain and, intriguingly, *mrs3*Δ *mrs4*Δ double mutation blocks growth of the P_{GAL1}-*IDP1*^{R148H} strain in YPGal and YEPEG media (Fig. 5A). Taken together, these data are in accord with a model in which *aco1*Δ-dependent and 2HG-mediated mtDNA loss occurs via distinct mechanisms. Because *mrs3*Δ *mrs4*Δ double mutation exacerbates P_{GAL1}-*IDP1*^{R148H}-dependent petite formation, this further supports the model that 2HG production interferes with mitochondrial iron homeostasis.

One mechanism by which citrate addition could suppress 2HG-mediated petite formation is by metabolism to α-ketoglutarate, thereby increasing intracellular levels of this key metabolite. Consistent with this hypothesis, the addition of dimethyl α-ketoglutarate (d-KG, a membrane-permeable derivative of α-ketoglutarate), significantly suppressed petite formation, resulting in an ∼50%-reduction in petite formation after 24 h of induction of the P_{GAL1}-*IDP1*^{R148H} strain (Fig. 5E). Because citrate and d-KG addition suppressed 2HG-mediated petite formation, we investigated if levels of α-ketoglutarate were reduced in the P_{GAL1}-*IDP1*^{R148H} strain as a consequence of both reduced isocitrate dehydrogenase activity and α-ketoglutarate conversion to 2HG. Consistent with this, we found a modest 20% reduction in α-ketoglutarate levels in the P_{GAL1}-*IDP1*^{R148H} strain (1.16 ± 0.06 μM) compared with the WT (1.42 ± 0.11 μM) and P_{GAL1}-*IDP1* (1.42 ± 0.26 μM) strains (Fig. 5D and Supplementary Material, Table S5).

Interestingly, we also observed petite formation in a heterozygous diploid strain with one WT *IDP1* gene and one mutant P_{GAL1}-*IDP1*^{R148H} allele (analogous to mammalian cancer-associated *IDH2*/*IDH2*^{R172X} genotypes), compared with *IDP1*/*IDP1* and *IDP1*/*idp1*Δ strains (Fig. 5F). Taken together, these results support the model that 2HG-production gain of function, rather than a net decrease in mitochondrial isocitrate dehydrogenase activity, is responsible for the deleterious mtDNA loss imparted by *IDP1*^{R148H} overexpression, and that the ratio of 2HG to α-ketoglutarate levels modulates 2HG toxicity.

Discussion

To provide new insights into the pathophysiological effects of how *IDH* mutations and the associated 2HG accumulation contribute to tumourigenesis, we introduced tumour-relevant mutations into the highly conserved yeast *IDP* genes. Strikingly, 2HG production following overexpression of the mutated mitochondrial *IDP1* resulted in high-level loss of mtDNA and respiratory function. Why does mutation of mitochondrial *IDP1*, but not the cytoplasmic *IDP2* isoform, and production of 2HG in the mitochondria, but not in the cytosol, result in loss of mtDNA? The mtDNA loss phenotype is likely not due to Idp1 exhibiting a dual role in mtDNA stability such as being a component of the mitochondrial nucleoid, as has been attributed to other mitochondrial enzymes, including Ilv5 (70) and Aco1 (66). If this were the case, we would expect a high degree of mtDNA loss in an *idp1*Δ strain, as observed for *ilv5*Δ and *aco1*Δ mutants, and that this is not observed argues against this dual role for Idp1. Instead, compartmentalization of metabolites may account for the differences in cytoplasmic versus mitochondrial 2HG production effects. To our knowledge, no information is available on the ability of 2HG to be transported across the mitochondrial membrane. 2HG produced in the cytoplasm may be readily transported into the mitochondria, and conversely, 2HG produced inside the mitochondria may not be easily transported out of the mitochondria to reduce mitochondrial levels. Even if trans-mitochondrial transport occurs, the 2HG concentration reached inside the mitochondria would be expected to be higher when it is produced inside the mitochondria than when it is produced in the cytoplasm. In addition, our data indicate that the toxicity of 2HG is likely related to the 2HG:α-ketoglutarate ratio. 2HG production will result in α-ketoglutarate consumption in the compartment it is produced in; thus, the mitochondrial 2HG:α-ketoglutarate ratio will be likely higher when 2HG is produced in the mitochondria than when it is transported into the mitochondria from the cytoplasm (if this indeed occurs).

We identified roles for genes involved in aldehyde dehydrogenation, iron homeostasis, and the retrograde response, in mitigating 2HG-mediated mtDNA damage.

Overexpression of the mitochondrial *ALD5* gene, which encodes a mitochondrial aldehyde dehydrogenase that converts acetaldehyde to acetyl-CoA and participates in the breakdown of toxic aldehydes accumulated during stress conditions, suppressed 2HG-mediated mtDNA loss in a role distinct from reducing 2HG levels. A role for Ald5 in respiratory metabolism and cytochrome c levels has also been reported, consistent with our results (71). Interestingly, like Idh1, Ald5 (and Ald4) also plays prominent roles in mitochondrial NADPH regeneration (72), which is important for the production of glutathione and protection against oxidative stress (73,74). Because NADPH levels are expected to be reduced in strains carrying *IDH1* 2HG-overproducing mutations, overexpression of *ALD5* could remediate the petite production phenotype by offsetting the NADPH deficit. While ROS-induced mtDNA damage is well-documented, we also did not observe suppression of petite formation by overexpression of the superoxide dismutase *SOD1* or *SOD2* genes, or supplementation with the antioxidant GSH. We also did not observe increased ROS formation upon 2HG production using a ROS-detection dye; however, physiologically relevant increases in ROS levels by 2HG production that were below the levels of detection in our experiment remain a possibility. Indeed, previous reports have documented a key function for both yeast and mammalian NADP isocitrate dehydrogenases in cellular defenses against oxidative-stress-induced damage (18,20,74). Ald5 shares extensive sequence identity (47%) with its human ortholog, the mitochondrial Aldh2, and its mutation is linked to carcinogenesis (75–77). If 2HG production also induces mtDNA loss in tumours, Aldh2 may provide an interesting candidate chemotherapeutic target for 2HG-producing cancers.

We present several lines of evidence that mitochondrial 2HG production perturbs iron homeostasis underscoring a role for cellular iron levels in the *IDP1*^{R148H}-mediated mtDNA loss and building upon the well-established intricate associations between iron homeostasis and mitochondrial function. Significantly, we observed that upon induction of 2HG production both iron levels and expression from the iron metabolon were elevated compared with the WT. Mutation of the mitochondrial iron transporter genes *MRS3* and *MRS4*, and of the iron utilization and homeostasis transcription factor gene *AFT1*, induced petite formation (Figs 4C and 5A). Conversely, high copy expression of the truncated *AFT1*$^{1\text{-}1207}$ allele, which

dampened expression of *FET3* and presumably other iron regulon genes, resulted in reduced cellular iron levels and suppressed petite formation. Furthermore, chelation of iron from the growth media suppressed petite formation. Increased iron levels in the mitochondria can damage mtDNA by reacting with oxygen metabolites to produce ROS (78). Mitochondria play important roles in the assembly of heme and iron sulphur clusters (ISC), and disruption of mtDNA results in reduced ISC assembly and Aft1-mediated induction of the iron regulon (79). Heme and ISC are important enzyme cofactors for redox reactions, such as respiratory electron transport, TCA cycle enzymes, DNA biosynthesis, as well as epigenetic modifications in mammalian cells, and these processes may all be dysregulated in cancers (80,81). Interestingly, α-ketoglutarate-dependent JmjC-domain histone demethylases and oxygenases that control HIF-1α are both thought to be inhibited by 2HG, and both require Fe(II) (22–24) and are readily inhibited by the iron chelator deferroxamine (15,82,83). Furthermore, glioblastoma stem-like cells require increased iron uptake and dependence for tumourigenesis, resulting in upregulation of the transferrin receptor and the iron chelator ferritin (45). Therefore, iron homeostasis and mitochondrial function are critical factors in tumourgenesis.

Defects in mtDNA and ISC assembly also induce retrograde signalling between the mitochondria and nucleus, which activates the expression of a subset of genes including TCA cycle genes such as *ACO1* and *CIT2* to increase TCA cycle intermediate and glutamate production (69). While disruption of the RTG response transcription factor *RTG1* suppressed mtDNA loss, we found no evidence that 2HG production activates the retrograde response. Although the pathway components differ, humans also possess a mitochondria-to-nuclear retrograde-type response stimulated via altered Ca^{2+} dynamics, and which activates ATF, NFAT and NFκB, to result in induction of glucose metabolism, oncogenesis, cell invasion, and anti-apoptotic genes (84–86).

By which other mechanisms might 2HG induce mtDNA loss? As discussed above, accumulated evidence indicates that 2HG competitively inhibits α-ketoglutarate-dependent enzymes by acting as a toxic α-ketoglutarate analog. Consistent with this model, citrate and d-KG may suppress the mtDNA loss observed here by being metabolized to α-ketoglutarate, and thereby elevating α-ketoglutarate levels to outcompete 2HG for substrate binding in a reaction important for mtDNA stability. Although the 2HG-targeting Tet family of DNA methylases and HIF-1α signalling are not conserved in yeast, Fe(II) and α-ketoglutarate-dependent chromatin-modifying JmjC histone demethylase orthologs are present (87), and 2HG perturbation of these could affect expression of nuclear genes that contribute to mtDNA stability.

Gliomas undergo substantially altered mtDNA gene copy number and large deletions, and these occur during the early stages of tumourigenesis (46–48). The mitochondria play an important role in apoptosis (88), to which gliomas are particularly resistant (89). Defects in oxidative respiration such as those caused by mtDNA damage can also result in metabolic rearrangements observed in most tumours known as the Warburg effect, whereby cancer cells shift to generate ATP mainly by glycolysis, followed by lactic acid oxidation in the cytosol instead of pyruvate oxidation in the mitochondria, to provide metabolites for anabolic metabolism (90). Mutations in the mitochondrial isoform sc*IDP1* (analogous to hs*IDH2*) gave rise to the loss of mtDNA, but this is not observed upon mutation of cytoplasmic sc*IDP2* (Fig. 1E) (analogous to hs*IDH1*, Fig. 1A). Although the incidence of mutations is higher in *IDH1* than in *IDH2* in gliomas, cholangiocarcinoma, and chondrosarcoma, they occur at similar frequencies in AML (6,91). Interestingly, although *IDH* mutations are correlated with a prolonged survival of glioma patients (1,92), this is not the case for AML patients (93). Therefore, it would be of interest to examine whether mtDNA loss is more prevalent in AML tumours, or whether mtDNA stability differs between *IDH1*- and *IDH2*-mutated tumours, in accord with our results. Our studies on the effects of oncometabolite 2HG production on mtDNA mutagenesis and loss, and the characterization of the mechanisms involved, provide a foundation for further studies using mammalian cancer models, and may contribute insights into possible prognostic indicators and novel approaches for cancer therapy.

Materials and Methods

Strains, media and growth conditions

Standard yeast culture media included Yeast Extract Peptone Dextrose (YPD), Yeast Extract Peptone Ethanol Glycerol (YEPEG), Yeast Extract Peptone Galactose (YPGal), Synthetic Dextrose (SD), Synthetic Galactose with no additional supplements (SGal), Synthetic Complete Galactose (SCGal), Synthetic Complete (SC), Synthetic Ethanol Glycerol (SEG), and YPGly 0.1% dextrose were prepared as described previously (94–98). YG-Ery media contained 20 g/l agar, 10 g/l yeast extract, 20 g/l glycerol, 50 mM sodium phosphate buffer (pH 6.5), and 4 g/l erythromycin (Sigma). Where specified media was supplemented with nourseothricin (Nat, 100 mg/l; Hans Knöll Institute für Naturstoff-Forschung, Jena, Germany), hygromycin B (Hyg, 300 mg/l; Calbiochem), G418 (geneticin, 200 mg/l; Life Technologies), 5-fluoroorotic acid (5-FOA, 1 g/l, Toronto Research Chemicals), dimethyl α-ketoglutarate (d-KG), l-canavanine (60 mg/l), bathophenanthroline disulfonate (BPS, Sigma), glutathione (GSH, Sigma) deferroxamine mesylate (DFO, Sigma). *S. cerevisiae* cultures were incubated at 30˚C.

S. cerevisiae strains used in this study were isogenic with S288c (99), and are listed in Supplementary Material, Table S1. The Rho^0 (lacking mtDNA) strain YJK3084 was obtained by passage three times on YPD + ethidium bromide (10 μg/ml) to eliminate the mitochondrial genome and confirmed by an inability to grow on YEPEG, and a lack of DAPI-stained mtDNA co-localizing with Mitotracker Red upon microscopic visualization of cells. Gene replacements and insertions with natMX4, kanMX4, hphMX4, or Ca*URA3* cassettes were constructed by PCR-mediated gene deletion (100–102). Strains containing *IDP* genes with tumour-relevant mutations under the control of the P_{GAL1} promoter were constructed via three consecutive transformations. First, the Ca*URA3* cassette was inserted into each gene to replace 3 bp at the region of mutation interest. Second, strains were co-transformed with a NAT-resistance selectable plasmid (pAG36) together with mutagenic oligonucleotides that contained ~40 bp homology on either side of the introduced mutation of interest. Following the loss of the marker plasmid, strains were plated onto SD + Ura + 5FOA media to select for replacement of the Ca*URA3* marker by the mutagenic oligonucleotide. Finally, hphMX4-P_{GAL1} or kanMX6-P_{GAL1}, amplified from pAG107 or pFA6a-kanMX6-P_{GAL1} using oligonucleotides also homologous to sequence upstream of the *IDP* genes, was introduced to replace 100 bp immediately upstream of the *IDP* ORF. Insertions and disruptions were confirmed by PCR and point mutations were also confirmed by sequencing. All oligonucleotides employed in this study are listed in Supplementary Material, Table S3.

Plasmid constructions

Plasmids employed in this study are listed in Supplementary Material, Table S2. Plasmids pJK1 and pJK8 were identified from a *URA3*-marked 2μm high-copy-number yeast genomic library containing 5- to 10-kb insertions within the SalI restriction site on plasmid pRS426 (constructed by C. Alarcon) and contained 6.1 and 3.2-kb inserts, respectively. To construct pJK5, *ALD5* in plasmid pJK1 was precisely replaced with the natMX4 cassette via PCR-mediated gene deletion. To construct pJK6, a PCR product containing *ALD5* together with 1 kb 5' and 0.5 kb 3' regions, flanked by pRS426-homologous sequence, was cloned into SalI/XhoI-linearized pRS426 by gap repair (103). Plasmid pJK46 containing the entire *AFT1* ORF together with 1 kb 5' and 0.5 kb 3' sequence was PCR-amplified using oligonucleotides that introduced NotI/SalI sites into the PCR product, and ligated into NotI/SalI-cleaved pRS426. Plasmid pJK52 was constructed from pJK8 following digestion with XhoI and religation, to eliminate *HSF1* sequence and retain partial *AFT1* (1.2 kb of 5' end) and 0.4 kb 5' sequence. Conversely, pJK53 was constructed following EcoRI-digestion of pJK8 and religation to eliminate *AFT1* sequence and retain partial (1.3 kb of 3' end) *HSF1* sequence. All plasmids were confirmed by restriction digestion analysis and sequencing.

Metabolite extraction

2HG was extracted from ~40 OD_{600nm} units of cells, grown for 6 h in galactose media to induce expression of the *IDP* genes under the control of the *GAL1* promoter. Cells were lysed by bead beating in 800 μl lysis buffer (50 mM Tris HCl, 100 mM KCl, 1 mM EDTA, 1% (v/v) Triton X) with 500 μl glass beads, for 8 bead beater cycles of 1.5 min interspersed with 1 min rest periods. Clarified lysates were normalized to protein concentration. Levels of 2HG were analysed by LC-negative electrospray ionization-MS/MS by the Duke University Pharmacokinetics/Pharmacodynamics core laboratory using previously described methods (104). Organic acids were extracted from 8 OD_{600nm} units of cells grown for 6 h in SCGal medium and analysed, as previously described (105). Extracts for analysis of iron levels were prepared in triplicate from ~$2x10^8$ cells and analyzed by ICP-MS (North Carolina State University, Raleigh), as described (106).

Microscopy

To visualize reactive oxygen (ROS) production, cells were stained with 10 μg/ml 2'7'-dichlorofluorescein diacetate (DCFH-DA; Sigma) and incubated for 2 h at 30˚C, as described previously (107). Fluorescence was counted for at least 100 cells from three independent cultures. As a positive control, cells were treated with 25 mM H_2O_2 for 1 hour at 30˚C prior to staining. To visualize mtDNA, cultures grown to log-phase were supplemented with 100 pM Mitotracker Red CMXRos (Molecular Probes), incubated for a further 50 min, and 10 nM 4',6-diamidino-2-phenylindole (DAPI, Sigma) was added for a further 5 min. Cells were twice-washed and visualized using a Zeiss Axioskop 2 Plus microscope using AxioVision 4.6 image acquisition software.

Fluctuation analysis of point mutations

To estimate rates of point mutation arising in the mitochondrial and nuclear genomes, fluctuation analyses were performed to assess spontaneous erythromycin resistance (Ery^R) and canavanine resistance (Can^R), respectively. For monitoring Ery^R, 10 independent colonies from YEPEG plates for each strain were inoculated and cultured in liquid YEPEG. Cells were harvested, washed, and used to inoculate 5 ml YPGal to $1x10^6$ cfu/ml. At 0 and 24 h incubation, approx 100-1000 and $1x10^8$ cfu were plated onto YEPEG and YG-Ery, to determine overall grande and Ery^R cfu, respectively. To assess the mutation rate to Can^R, 10 independent colonies for each strain were inoculated into SC-Arg, cultured overnight, washed, and used as an inoculum for 5 ml YPGal to $1x10^5$ cfu/ml. At 0 and 42-h incubation, approximately 100 and $3x10^7$ cfu were plated on YPD and SC-arg + canavanine to estimate overall viable and Can^R cfu, respectively. The analysis of the mean was determined using the Luria-Delbrück fluctuation analysis calculator (FALCOR) web tool (108).

Determination of respiration loss frequency

To determine the percentage of nonrespiring cells in the population, strains were first cultured in YEPEG or SEG to ensure all growing cells were respiration-competent. Cells were washed two times with water and inoculated into YPGal or SCGal-Ura (at ~$1x10^4$ cfu/ml) and following incubation for 0, 24, and 48 h, cells were diluted and plated onto YPGly 0.1% dextrose. Following 5 days incubation, colonies were scored for respiration competence based on differential colony size morphology (97).

Whole genome sequencing and assembly

DNA for whole genome sequencing was extracted as described previously (109). Whole genome sequencing was performed on the Hiseq2500 platform by the UNC Next Generation Sequencing Facility. Paired end libraries with approximately 300 base inserts were prepared and multiplexed with 24 samples to a single lane. The Illumina pipeline (v.1.8.2) was used for initial processing of raw data. Sequences have been deposited to the Sequence Read Archive under project accession number PRJNA306764. Sequences were mapped to the S288c reference genome (110) using the short read component of the BWA aligner (111). Realignment and SNP calling were performed using the Genome Analysis Toolkit's Unified Genotyper (112) with the haploid ploidy setting as per the pipeline version 2.4-9. This pipeline also utilized both Picard and SAMtools (113). Depth of coverage was also determined using SAMtools and plotted using R (114). Variant filtering was performed using VCFtools (115) and SNP impact was inferred using SnpEff (116).

Quantitative Real-Time PCR analysis

RNA was extracted from 20-30 OD_{600nm} units of cells using a Qiagen RNeasy kit and DNAse-treated (Ambion). RNA transcripts were reverse-transcribed using AffinityScript RT-RNase (Agilent Technologies). Quantitative Real-Time PCR (RT-PCR) assays were performed with an Applied Biosystems 7500 Real-Time PCR System using Brilliant SYBR Green qRT-PCR master mix (Agilent Technologies). The data were analysed using StepOne™ Software v2.1 (Life Technologies).

Supplementary Material

Supplementary Material is available at *HMG* online.

Acknowledgements

The authors are indebted to Olga Ilkayeva and Chris Newgard and the Duke Molecular Physiology Institute metabolomics core laboratory for metabolomic analyses. We thank Kim Hutchison for running ICP-MS samples at North Carolina State University, Raleigh. We also gratefully acknowledge Hai Yan, Elaine Sia, Julian Rutherford, Dennis Thiele, and Richard Festa for helpful discussions, as well as Jerry Kaplan, David Eide, and Valeria Culotta for providing plasmids.

Conflict of Interest Statement. None declared.

Funding

Funding was provided by the National Institutes of Health (grant numbers R01-CA154499 awarded to MEC; P01-AI104533 and R01-AI112595 awarded to JH).

References

1. Parsons, D.W., Jones, S., Zhang, X., Lin, J.C., Leary, R.J., Angenendt, P., Mankoo, P., Carter, H., Siu, I.M., Gallia, G.L., *et al.* (2008) An integrated genomic analysis of human glioblastoma multiforme. *Science*, **321**, 1807–1812.
2. Yan, H., Parsons, D.W., Jin, G., McLendon, R., Rasheed, B.A., Yuan, W., Kos, I., Batinic-Haberle, I., Jones, S., Riggins, G.J., *et al.* (2009) *IDH1* and *IDH2* mutations in gliomas. *N. Engl. J. Med.*, **360**, 765–773.
3. Bleeker, F.E., Lamba, S., Leenstra, S., Troost, D., Hulsebos, T., Vandertop, W.P., Frattini, M., Molinari, F., Knowles, M., Cerrato, A., *et al.* (2009) *IDH1* mutations at residue p.R132 (*IDH1R132*) occur frequently in high-grade gliomas but not in other solid tumors. *Hum. Mutat.*, **30**, 7–11.
4. Hartmann, C., Meyer, J., Balss, J., Capper, D., Mueller, W., Christians, A., Felsberg, J., Wolter, M., Mawrin, C., Wick, W., *et al.* (2009) Type and frequency of *IDH1* and *IDH2* mutations are related to astrocytic and oligodendroglial differentiation and age: a study of 1,010 diffuse gliomas. *Acta Neuropathol.*, **118**, 469–474.
5. Mardis, E.R., Ding, L., Dooling, D.J., Larson, D.E., McLellan, M.D., Chen, K., Koboldt, D.C., Fulton, R.S., Delehaunty, K.D., McGrath, S.D., *et al.* (2009) Recurring mutations found by sequencing an acute myeloid leukemia genome. *N. Engl. J. Med.*, **361**, 1058–1066.
6. Ward, P.S., Patel, J., Wise, D.R., Abdel-Wahab, O., Bennett, B.D., Coller, H.A., Cross, J.R., Fantin, V.R., Hedvat, C.V., Perl, A.E., *et al.* (2010) The common feature of leukemia-associated *IDH1* and *IDH2* mutations is a neomorphic enzyme activity converting alpha-ketoglutarate to 2-hydroxyglutarate. *Cancer Cell*, **17**, 225–234.
7. Green, A., and Beer, P. (2010) Somatic mutations of *IDH1* and *IDH2* in the leukemic transformation of myeloproliferative neoplasms. *N. Engl. J. Med.*, **362**, 369–370.
8. Green, C.L., Evans, C.M., Zhao, L., Hills, R.K., Burnett, A.K., Linch, D.C., and Gale, R.E. (2011) The prognostic significance of *IDH2* mutations depends on the location of the mutation. *Blood*, **118**, 409–412.
9. Amary, M.F., Bacsi, K., Maggiani, F., Damato, S., Halai, D., Berisha, F., Pollock, R., O'Donnell, P., Grigoriadis, A., Diss, T., *et al.* (2011) *IDH1* and *IDH2* mutations are frequent events in central chondrosarcoma and central and periosteal chondromas but not in other mesenchymal tumours. *J. Pathol.*, **224**, 334–343.
10. Pansuriya, T.C., van Eijk, R., d'Adamo, P., van Ruler, M.A., Kuijjer, M.L., Oosting, J., Cleton-Jansen, A.M., van Oosterwijk, J.G., Verbeke, S.L., Meijer, D., *et al.* (2011) Somatic mosaic *IDH1* and *IDH2* mutations are associated with enchondroma and spindle cell hemangioma in Ollier disease and Maffucci syndrome. *Nat. Genet.*, **43**, 1256–1261.
11. Xu, X., Zhao, J., Xu, Z., Peng, B., Huang, Q., Arnold, E., and Ding, J. (2004) Structures of human cytosolic NADP-dependent isocitrate dehydrogenase reveal a novel self-regulatory mechanism of activity. *J. Biol. Chem.*, **279**, 33946–33957.
12. Zhao, S., Lin, Y., Xu, W., Jiang, W., Zha, Z., Wang, P., Yu, W., Li, Z., Gong, L., Peng, Y., *et al.* (2009) Glioma-derived mutations in *IDH1* dominantly inhibit IDH1 catalytic activity and induce HIF-1alpha. *Science*, **324**, 261–265.
13. Dang, L., White, D.W., Gross, S., Bennett, B.D., Bittinger, M.A., Driggers, E.M., Fantin, V.R., Jang, H.G., Jin, S., Keenan, M.C., *et al.* (2009) Cancer-associated *IDH1* mutations produce 2-hydroxyglutarate. *Nature*, **462**, 739–744.
14. Gross, S., Cairns, R.A., Minden, M.D., Driggers, E.M., Bittinger, M.A., Jang, H.G., Sasaki, M., Jin, S., Schenkein, D.P., Su, S.M., *et al.* (2010) Cancer-associated metabolite 2-hydroxyglutarate accumulates in acute myelogenous leukemia with isocitrate dehydrogenase 1 and 2 mutations. *J. Exp. Med.*, **207**, 339–344.
15. Schofield, C.J., and Ratcliffe, P.J. (2004) Oxygen sensing by HIF hydroxylases. *Nat. Rev. Mol. Cell Biol.*, **5**, 343–354.
16. MacKenzie, E.D., Selak, M.A., Tennant, D.A., Payne, L.J., Crosby, S., Frederiksen, C.M., Watson, D.G., and Gottlieb, E. (2007) Cell-permeating alpha-ketoglutarate derivatives alleviate pseudohypoxia in succinate dehydrogenase-deficient cells. *Mol. Cell. Biol.*, **27**, 3282–3289.
17. Thompson, C.B. (2009) Metabolic enzymes as oncogenes or tumor suppressors. *N. Engl. J. Med.*, **360**, 813–815.
18. Lee, S.M., Koh, H.J., Park, D.C., Song, B.J., Huh, T.L., and Park, J.W. (2002) Cytosolic NADP(+)-dependent isocitrate dehydrogenase status modulates oxidative damage to cells. *Free Radic. Biol. Med.*, **32**, 1185–1196.
19. Nakamura, H. (2005) Thioredoxin and its related molecules: update 2005. *Antioxid. Redox Signal.*, **7**, 823–828.
20. Kim, S.Y., Lee, S.M., Tak, J.K., Choi, K.S., Kwon, T.K., and Park, J.W. (2007) Regulation of singlet oxygen-induced apoptosis by cytosolic NADP+-dependent isocitrate dehydrogenase. *Mol. Cell. Biochem.*, **302**, 27–34.
21. Frezza, C., Tennant, D.A., and Gottlieb, E. (2010) *IDH1* mutations in gliomas: when an enzyme loses its grip. *Cancer Cell*, **17**, 7–9.
22. Chowdhury, R., Yeoh, K.K., Tian, Y.M., Hillringhaus, L., Bagg, E.A., Rose, N.R., Leung, I.K., Li, X.S., Woon, E.C., Yang, M., *et al.* (2011) The oncometabolite 2-hydroxyglutarate inhibits histone lysine demethylases. *EMBO Rep.*, **12**, 463–469.
23. Xu, W., Yang, H., Liu, Y., Yang, Y., Wang, P., Kim, S.H., Ito, S., Yang, C., Xiao, M.T., Liu, L.X., *et al.* (2011) Oncometabolite 2-hydroxyglutarate is a competitive inhibitor of alpha-ketoglutarate-dependent dioxygenases. *Cancer Cell*, **19**, 17–30.
24. Figueroa, M.E., Abdel-Wahab, O., Lu, C., Ward, P.S., Patel, J., Shih, A., Li, Y., Bhagwat, N., Vasanthakumar, A., Fernandez, H.F., *et al.* (2010) Leukemic *IDH1* and *IDH2* mutations result in a hypermethylation phenotype, disrupt TET2 function, and impair hematopoietic differentiation. *Cancer Cell*, **18**, 553–567.
25. Noushmehr, H., Weisenberger, D.J., Diefes, K., Phillips, H.S., Pujara, K., Berman, B.P., Pan, F., Pelloski, C.E., Sulman, E.P., Bhat, K.P., *et al.* (2010) Identification of a CpG island

methylator phenotype that defines a distinct subgroup of glioma. *Cancer Cell*, **17**, 510–522.
26. Christensen, B.C., Smith, A.A., Zheng, S., Koestler, D.C., Houseman, E.A., Marsit, C.J., Wiemels, J.L., Nelson, H.H., Karagas, M.R., Wrensch, M.R., *et al.* (2011) DNA methylation, isocitrate dehydrogenase mutation, and survival in glioma. *J. Natl. Cancer Inst.*, **103**, 143–153.
27. Laffaire, J., Everhard, S., Idbaih, A., Criniere, E., Marie, Y., de Reynies, A., Schiappa, R., Mokhtari, K., Hoang-Xuan, K., Sanson, M., *et al.* (2011) Methylation profiling identifies 2 groups of gliomas according to their tumorigenesis. *Neuro Oncol.*, **13**, 84–98.
28. Duncan, C.G., Barwick, B.G., Jin, G., Rago, C., Kapoor-Vazirani, P., Powell, D.R., Chi, J.T., Bigner, D.D., Vertino, P.M., and Yan, H. (2012) A heterozygous *IDH1R132H/WT* mutation induces genome-wide alterations in DNA methylation. *Genome Res.*, **22**, 2339–2355.
29. Jones, P.A., and Baylin, S.B. (2007) The epigenomics of cancer. *Cell*, **128**, 683–692.
30. von Deimling, A., Korshunov, A., and Hartmann, C. (2011) The next generation of glioma biomarkers: MGMT methylation, BRAF fusions and *IDH1* mutations. *Brain Pathol.*, **21**, 74–87.
31. Watanabe, T., Nobusawa, S., Kleihues, P., and Ohgaki, H. (2009) *IDH1* mutations are early events in the development of astrocytomas and oligodendrogliomas. *Am. J. Pathol.*, **174**, 1149–1153.
32. Ichimura, K., Pearson, D.M., Kocialkowski, S., Backlund, L.M., Chan, R., Jones, D.T., and Collins, V.P. (2009) *IDH1* mutations are present in the majority of common adult gliomas but rare in primary glioblastomas. *Neuro Oncol.*, **11**, 341–347.
33. Labussiere, M., Idbaih, A., Wang, X.W., Marie, Y., Boisselier, B., Falet, C., Paris, S., Laffaire, J., Carpentier, C., Criniere, E., *et al.* (2010) All the 1p19q codeleted gliomas are mutated on *IDH1* or *IDH2*. *Neurology*, **74**, 1886–1890.
34. Nekrutenko, A., Hillis, D.M., Patton, J.C., Bradley, R.D., and Baker, R.J. (1998) Cytosolic isocitrate dehydrogenase in humans, mice, and voles and phylogenetic analysis of the enzyme family. *Mol. Biol. Evol.*, **15**, 1674–1684.
35. Haselbeck, R.J., and McAlister-Henn, L. (1993) Function and expression of yeast mitochondrial NAD- and NADP-specific isocitrate dehydrogenases. *J. Biol. Chem.*, **268**, 12116–12122.
36. Zhao, W.N., and McAlister-Henn, L. (1996) Expression and gene disruption analysis of the isocitrate dehydrogenase family in yeast. *Biochemistry*, **35**, 7873–7878.
37. Contreras-Shannon, V., Lin, A.P., McCammon, M.T., and McAlister-Henn, L. (2005) Kinetic properties and metabolic contributions of yeast mitochondrial and cytosolic NADP+-specific isocitrate dehydrogenases. *J. Biol. Chem.*, **280**, 4469–4475.
38. Lu, Q., and McAlister-Henn, L. (2010) Peroxisomal localization and function of NADP+ -specific isocitrate dehydrogenases in yeast. *Arch. Biochem. Biophys.*, **493**, 125–134.
39. Henke, B., Girzalsky, W., Berteaux-Lecellier, V., and Erdmann, R. (1998) *IDP3* encodes a peroxisomal NADP-dependent isocitrate dehydrogenase required for the beta-oxidation of unsaturated fatty acids. *J. Biol. Chem.*, **273**, 3702–3711.
40. Minard, K.I., and McAlister-Henn, L. (1999) Dependence of peroxisomal beta-oxidation on cytosolic sources of NADPH. *J. Biol. Chem.*, **274**, 3402–3406.
41. Minard, K.I., and McAlister-Henn, L. (2001) Antioxidant function of cytosolic sources of NADPH in yeast. *Free Radic. Biol. Med.*, **31**, 832–843.
42. DeRisi, J.L., Iyer, V.R., and Brown, P.O. (1997) Exploring the metabolic and genetic control of gene expression on a genomic scale. *Science*, **278**, 680–686.
43. Minard, K.I., Jennings, G.T., Loftus, T.M., Xuan, D., and McAlister-Henn, L. (1998) Sources of NADPH and expression of mammalian NADP+-specific isocitrate dehydrogenases in *Saccharomyces cerevisiae*. *J. Biol. Chem.*, **273**, 31486–31493.
44. Lu, Q., Minard, K.I., and McAlister-Henn, L. (2008) Dual compartmental localization and function of mammalian NADP+-specific isocitrate dehydrogenase in yeast. *Arch. Biochem. Biophys.*, **472**, 17–25.
45. Schonberg, D.L., Miller, T.E., Wu, Q., Flavahan, W.A., Das, N.K., Hale, J.S., Hubert, C.G., Mack, S.C., Jarrar, A.M., Karl, R.T., *et al.* (2015) Preferential iron trafficking characterizes glioblastoma stem-like cells. *Cancer Cell*, **28**, 441–455.
46. Liang, B.C., and Hays, L. (1996) Mitochondrial DNA copy number changes in human gliomas. *Cancer Lett.*, **105**, 167–173.
47. Liang, B.C. (1996) Evidence for association of mitochondrial DNA sequence amplification and nuclear localization in human low-grade gliomas. *Mutat. Res.*, **354**, 27–33.
48. Kirches, E., Michael, M., Woy, C., Schneider, T., Warich-Kirches, M., Schneider-Stock, R., Winkler, K., Wittig, H., and Dietzmann, K. (1999) Loss of heteroplasmy in the displacement loop of brain mitochondrial DNA in astrocytic tumors. *Genes Chromosomes Cancer*, **26**, 80–83.
49. Longo, V.D., Gralla, E.B., and Valentine, J.S. (1996) Superoxide dismutase activity is essential for stationary phase survival in *Saccharomyces cerevisiae*. Mitochondrial production of toxic oxygen species *in vivo*. *J. Biol. Chem.*, **271**, 12275–12280.
50. Bohr, V.A. (2002) Repair of oxidative DNA damage in nuclear and mitochondrial DNA, and some changes with aging in mammalian cells. *Free Radic. Biol. Med.*, **32**, 804–812.
51. Fendt, S.M., and Sauer, U. (2010) Transcriptional regulation of respiration in yeast metabolizing differently repressive carbon substrates. *BMC Syst. Biol.*, **4**, 12.
52. Jamieson, D.J. (1998) Oxidative stress responses of the yeast *Saccharomyces cerevisiae*. *Yeast*, **14**, 1511–1527.
53. Whelan, W.L., Gocke, E., and Manney, T.R. (1979) The *CAN1* locus of *Saccharomyces cerevisiae*: fine-structure analysis and forward mutation rates. *Genetics*, **91**, 35–51.
54. Sor, F., and Fukuhara, H. (1982) Identification of two erythromycin resistance mutations in the mitochondrial gene coding for the large ribosomal RNA in yeast. *Nucleic Acids Res.*, **10**, 6571–6577.
55. Sor, F., and Fukuhara, H. (1984) Erythromycin and spiramycin resistance mutations of yeast mitochondria: nature of the *rib2* locus in the large ribosomal RNA gene. *Nucleic Acids Res.*, **12**, 8313–8318.
56. Pogorzala, L., Mookerjee, S., and Sia, E.A. (2009) Evidence that Msh1p plays multiple roles in mitochondrial base excision repair. *Genetics*, **182**, 699–709.
57. Aranda, A., and del Olmo Ml, M. (2003) Response to acetaldehyde stress in the yeast *Saccharomyces cerevisiae* involves a strain-dependent regulation of several *ALD* genes and is mediated by the general stress response pathway. *Yeast*, **20**, 747–759.
58. Casas, C., Aldea, M., Espinet, C., Gallego, C., Gil, R., and Herrero, E. (1997) The *AFT1* transcriptional factor is differentially required for expression of high-affinity iron uptake genes in *Saccharomyces cerevisiae*. *Yeast*, **13**, 621–637.

59. Yamaguchi-Iwai, Y., Stearman, R., Dancis, A., and Klausner, R.D. (1996) Iron-regulated DNA binding by the AFT1 protein controls the iron regulon in yeast. *Embo J.*, **15**, 3377–3384.
60. Yamaguchi-Iwai, Y., Dancis, A., and Klausner, R.D. (1995) *AFT1*: a mediator of iron regulated transcriptional control in *Saccharomyces cerevisiae*. *Embo J.*, **14**, 1231–1239.
61. Dimmer, K.S., Fritz, S., Fuchs, F., Messerschmitt, M., Weinbach, N., Neupert, W., and Westermann, B. (2002) Genetic basis of mitochondrial function and morphology in *Saccharomyces cerevisiae*. *Mol. Biol. Cell*, **13**, 847–853.
62. Merz, S., and Westermann, B. (2009) Genome-wide deletion mutant analysis reveals genes required for respiratory growth, mitochondrial genome maintenance and mitochondrial protein synthesis in *Saccharomyces cerevisiae*. *Genome Biol.*, **10**, R95.
63. Jeong, M.Y., Kang, C.M., Kim, J.H., Heo, D.H., Chang, M., Baek, I.J., Ro, H.S., Choi, I.D., Kim, T.H., and Yun, C.W. (2009) A novel function of Aft1 in regulating ferrioxamine B uptake: Aft1 modulates Arn3 ubiquitination in *Saccharomyces cerevisiae*. *Biochem. J.*, **422**, 181–191.
64. Yun, C.W., Ferea, T., Rashford, J., Ardon, O., Brown, P.O., Botstein, D., Kaplan, J., and Philpott, C.C. (2000) Desferrioxamine-mediated iron uptake in *Saccharomyces cerevisiae*. Evidence for two pathways of iron uptake. *J. Biol. Chem.*, **275**, 10709–10715.
65. McCammon, M.T., Epstein, C.B., Przybyla-Zawislak, B., McAlister-Henn, L., and Butow, R.A. (2003) Global transcription analysis of Krebs tricarboxylic acid cycle mutants reveals an alternating pattern of gene expression and effects on hypoxic and oxidative genes. *Mol. Biol. Cell*, **14**, 958–972.
66. Chen, X.J., Wang, X., Kaufman, B.A., and Butow, R.A. (2005) Aconitase couples metabolic regulation to mitochondrial DNA maintenance. *Science*, **307**, 714–717.
67. Lin, A.P., Hakala, K.W., Weintraub, S.T., and McAlister-Henn, L. (2008) Suppression of metabolic defects of yeast isocitrate dehydrogenase and aconitase mutants by loss of citrate synthase. *Arch. Biochem. Biophys.*, **474**, 205–212.
68. Farooq, M.A., Pracheil, T.M., Dong, Z., Xiao, F., and Liu, Z. (2013) Mitochondrial DNA instability in cells lacking aconitase correlates with iron citrate toxicity. *Oxid. Med. Cell. Longev.*, **2013**, 493536.
69. Liu, Z., and Butow, R.A. (2006) Mitochondrial retrograde signaling. *Annu. Rev. Genet.*, **40**, 159–185.
70. Zelenaya-Troitskaya, O., Perlman, P.S., and Butow, R.A. (1995) An enzyme in yeast mitochondria that catalyzes a step in branched-chain amino acid biosynthesis also functions in mitochondrial DNA stability. *Embo J.*, **14**, 3268–3276.
71. Kurita, O., and Nishida, Y. (1999) Involvement of mitochondrial aldehyde dehydrogenase *ALD5* in maintenance of the mitochondrial electron transport chain in *Saccharomyces cerevisiae*. *FEMS Microbiol. Lett.*, **181**, 281–287.
72. Miyagi, H., Kawai, S., and Murata, K. (2009) Two sources of mitochondrial NADPH in the yeast *Saccharomyces cerevisiae*. *J. Biol. Chem.*, **284**, 7553–7560.
73. Pollak, N., Dolle, C., and Ziegler, M. (2007) The power to reduce: pyridine nucleotides–small molecules with a multitude of functions. *Biochem. J.*, **402**, 205–218.
74. Jo, S.H., Son, M.K., Koh, H.J., Lee, S.M., Song, I.H., Kim, Y.O., Lee, Y.S., Jeong, K.S., Kim, W.B., Park, J.W., *et al.* (2001) Control of mitochondrial redox balance and cellular defense against oxidative damage by mitochondrial NADP+-dependent isocitrate dehydrogenase. *J. Biol. Chem.*, **276**, 16168–16176.
75. Lindahl, R. (1992) Aldehyde dehydrogenases and their role in carcinogenesis. *Crit. Rev. Biochem. Mol. Biol.*, **27**, 283–335.
76. Yoshida, A., Rzhetsky, A., Hsu, L.C., and Chang, C. (1998) Human aldehyde dehydrogenase gene family. *Eur. J. Biochem.*, **251**, 549–557.
77. Kamino, K., Nagasaka, K., Imagawa, M., Yamamoto, H., Yoneda, H., Ueki, A., Kitamura, S., Namekata, K., Miki, T., and Ohta, S. (2000) Deficiency in mitochondrial aldehyde dehydrogenase increases the risk for late-onset Alzheimer's disease in the Japanese population. *Biochem. Biophys. Res. Commun.*, **273**, 192–196.
78. Kaniak-Golik, A., and Skoneczna, A. (2015) Mitochondria-nucleus network for genome stability. *Free Radic. Biol. Med.*, **82**, 73–104.
79. Veatch, J.R., McMurray, M.A., Nelson, Z.W., and Gottschling, D.E. (2009) Mitochondrial dysfunction leads to nuclear genome instability via an iron-sulfur cluster defect. *Cell*, **137**, 1247–1258.
80. Torti, S.V., and Torti, F.M. (2013) Iron and cancer: more ore to be mined. *Nat. Rev. Cancer*, **13**, 342–355.
81. Lane, D.J., Mills, T.M., Shafie, N.H., Merlot, A.M., Saleh Moussa, R., Kalinowski, D.S., Kovacevic, Z., and Richardson, D.R. (2014) Expanding horizons in iron chelation and the treatment of cancer: role of iron in the regulation of ER stress and the epithelial-mesenchymal transition. *Biochim Biophys Acta*, **1845**, 166–181.
82. Koehntop, K.D., Emerson, J.P., and Que, L. Jr. (2005) The 2-His-1-carboxylate facial triad: a versatile platform for dioxygen activation by mononuclear non-heme iron(II) enzymes. *J. Biol. Inorg. Chem.*, **10**, 87–93.
83. Whetstine, J.R., Nottke, A., Lan, F., Huarte, M., Smolikov, S., Chen, Z., Spooner, E., Li, E., Zhang, G., Colaiacovo, M., *et al.* (2006) Reversal of histone lysine trimethylation by the JMJD2 family of histone demethylases. *Cell*, **125**, 467–481.
84. Butow, R.A., and Avadhani, N.G. (2004) Mitochondrial signaling: the retrograde response. *Mol. Cell*, **14**, 1–15.
85. Biswas, G., Guha, M., and Avadhani, N.G. (2005) Mitochondria-to-nucleus stress signaling in mammalian cells: nature of nuclear gene targets, transcription regulation, and induced resistance to apoptosis. *Gene*, **354**, 132–139.
86. Wallace, D.C. (2012) Mitochondria and cancer. *Nat. Rev. Cancer*, **12**, 685–698.
87. Tsukada, Y., Fang, J., Erdjument-Bromage, H., Warren, M.E., Borchers, C.H., Tempst, P., and Zhang, Y. (2006) Histone demethylation by a family of JmjC domain-containing proteins. *Nature*, **439**, 811–816.
88. Wang, X. (2001) The expanding role of mitochondria in apoptosis. *Genes Dev.*, **15**, 2922–2933.
89. Maher, E.A., Furnari, F.B., Bachoo, R.M., Rowitch, D.H., Louis, D.N., Cavenee, W.K., and DePinho, R.A. (2001) Malignant glioma: genetics and biology of a grave matter. *Genes Dev.*, **15**, 1311–1333.
90. Warburg, O. (1956) On the origin of cancer cells. *Science*, **123**, 309–314.
91. Molenaar, R.J., Radivoyevitch, T., Maciejewski, J.P., van Noorden, C.J., and Bleeker, F.E. (2014) The driver and passenger effects of isocitrate dehydrogenase 1 and 2 mutations in oncogenesis and survival prolongation. *Biochim. Biophys. Acta*, **1846**, 326–341.

92. Sanson, M., Marie, Y., Paris, S., Idbaih, A., Laffaire, J., Ducray, F., El Hallani, S., Boisselier, B., Mokhtari, K., Hoang-Xuan, K., *et al.* (2009) Isocitrate dehydrogenase 1 codon 132 mutation is an important prognostic biomarker in gliomas. *J. Clin. Oncol.*, **27**, 4150–4154.
93. Abbas, S., Lugthart, S., Kavelaars, F.G., Schelen, A., Koenders, J.E., Zeilemaker, A., van Putten, W.J., Rijneveld, A.W., Lowenberg, B., and Valk, P.J. (2010) Acquired mutations in the genes encoding IDH1 and IDH2 both are recurrent aberrations in acute myeloid leukemia: prevalence and prognostic value. *Blood*, **116**, 2122–2126.
94. Sherman, F., Fink, G.R.,. and Lawrence, C.W. (1974) *Methods in Yeast Genetics*. Cold Spring Harbor Laboratory, Cold Spring Harbor.
95. Sambrook, J., Fritsch, E.F. and Maniatis, T. (1989) *Molecular cloning: A laboratory manual*. Cold Spring Harbor Laboratory Press, Cold Spring Harbor, New York.
96. Ito-Harashima, S., Hartzog, P.E., Sinha, H., and McCusker, J.H. (2002) The tRNA-Tyr gene family of *Saccharomyces cerevisiae*: agents of phenotypic variation and position effects on mutation frequency. *Genetics*, **161**, 1395–1410.
97. Mookerjee, S.A., Lyon, H.D., and Sia, E.A. (2005) Analysis of the functional domains of the mismatch repair homologue Msh1p and its role in mitochondrial genome maintenance. *Curr. Genet.*, **47**, 84–99.
98. Kingsbury, J.M., and McCusker, J.H. (2010) Cytocidal amino acid starvation of *Saccharomyces cerevisiae* and *Candida albicans* acetolactate synthase (*ilv2*Δ) mutants is influenced by the carbon source and rapamycin. *Microbiology*, **156**, 929–939.
99. Mortimer, R.K., and Johnston, J.R. (1986) Genealogy of principal strains of the yeast genetic stock center. *Genetics*, **113**, 35–43.
100. Wach, A., Brachat, A., Pohlmann, R., and Philippsen, P. (1994) New heterologous modules for classical or PCR-based gene disruptions in *Saccharomyces cerevisiae*. *Yeast*, **10**, 1793–1808.
101. Goldstein, A.L., and McCusker, J.H. (1999) Three new dominant drug resistance cassettes for gene disruption in *Saccharomyces cerevisiae*. *Yeast*, **15**, 1541–1553.
102. Goldstein, A.L., Pan, X., and McCusker, J.H. (1999) Heterologous URA3MX cassettes for gene replacement in *Saccharomyces cerevisiae*. *Yeast*, **15**, 507–511.
103. Oldenburg, K.R., Vo, K.T., Michaelis, S., and Paddon, C. (1997) Recombination-mediated PCR-directed plasmid construction *in vivo* in yeast. *Nucleic Acids Res.*, **25**, 451–452.
104. Jin, G., Reitman, Z.J., Spasojevic, I., Batinic-Haberle, I., Yang, J., Schmidt-Kittler, O., Bigner, D.D., and Yan, H. (2011) 2-hydroxyglutarate production, but not dominant negative function, is conferred by glioma-derived NADP-dependent isocitrate dehydrogenase mutations. *PLoS One*, **6**, e16812.
105. Kingsbury, J.M., Sen, N.D., and Cardenas, M.E. (2015) Branched-chain aminotransferases control TORC1 signaling in *Saccharomyces cerevisiae*. *PLoS Genet.*, **11**, e1005714.
106. Festa, R.A., Helsel, M.E., Franz, K.J., and Thiele, D.J. (2014) Exploiting innate immune cell activation of a copper-dependent antimicrobial agent during infection. *Chem. Biol.*, **21**, 977–987.
107. Lee, Y.J., Hoe, K.L., and Maeng, P.J. (2007) Yeast cells lacking the *CIT1*-encoded mitochondrial citrate synthase are hypersusceptible to heat- or aging-induced apoptosis. *Mol. Biol. Cell*, **18**, 3556–3567.
108. Hall, B.M., Ma, C.X., Liang, P., and Singh, K.K. (2009) Fluctuation analysis CalculatOR: a web tool for the determination of mutation rate using Luria-Delbruck fluctuation analysis. *Bioinformatics*, **25**, 1564–1565.
109. Pitkin, J.W., Panaccione, D.G., and Walton, J.D. (1996) A putative cyclic peptide efflux pump encoded by the *TOXA* gene of the plant-pathogenic fungus *Cochliobolus carbonum*. *Microbiology*, **142**, 1557–1565.
110. Goffeau, A., Barrell, B.G., Bussey, H., Davis, R.W., Dujon, B., Feldmann, H., Galibert, F., Hoheisel, J.D., Jacq, C., Johnston, M., *et al.* (1996) Life with 6000 genes. *Science*, **274**, 546, 563–547.
111. Li, H., and Durbin, R. (2009) Fast and accurate short read alignment with Burrows-Wheeler transform. *Bioinformatics*, **25**, 1754–1760.
112. McKenna, A., Hanna, M., Banks, E., Sivachenko, A., Cibulskis, K., Kernytsky, A., Garimella, K., Altshuler, D., Gabriel, S., Daly, M., *et al.* (2010) The Genome Analysis Toolkit: a MapReduce framework for analyzing next-generation DNA sequencing data. *Genome Res.*, **20**, 1297–1303.
113. Li, H., Handsaker, B., Wysoker, A., Fennell, T., Ruan, J., Homer, N., Marth, G., Abecasis, G., and Durbin, R. and Genome Project Data Processing Subgroup (2009) The Sequence Alignment/Map format and SAMtools. *Bioinformatics*, **25**, 2078–2079.
114. Team, R.D.C (2005) *R: A language and environment for statistical computing*. R Foundation for Statistical Computing, Vienna, Austria
115. Danecek, P., Auton, A., Abecasis, G., Albers, C.A., Banks, E., DePristo, M.A., Handsaker, R.E., Lunter, G., Marth, G.T., Sherry, S.T., *et al.* (2011) The variant call format and VCFtools. *Bioinformatics*, **27**, 2156–2158.
116. Cingolani, P., Platts, A., Wang le, L., Coon, M., Nguyen, T., Wang, L., Land, S.J., Lu, X., and Ruden, D.M. (2012) A program for annotating and predicting the effects of single nucleotide polymorphisms, SnpEff: SNPs in the genome of *Drosophila melanogaster* strain w1118; iso-2; iso-3. *Fly (Austin)*, **6**, 80–92.